

# Frenetic steering: nonequilibrium-enabled navigation

Bram Lefebvre and Christian Maes

Department of Physics and Astronomy, KU Leuven, B-3001 Leuven, Belgium,\*

We explain the steering of slow degrees of freedom by coupling them to driven components for which the time-symmetric reactivities are manipulated. We present the strategy and main principle that make that sort of navigation feasible. For illustration, nonlinear limit cycles (as in the van der Pol oscillator) and strange attractors (as in the Lorenz dynamics) are seen to emerge when the driving in the nonequilibrium medium is kept fixed while the frenesy is tuned to produce the required forces. We imagine that such frenetic control is available in Life as well, allowing selection of the appropriate biological functioning.

Keywords: nonequilibrium; frenesy; control theory; slow/fast dynamical systems

## Significance

The paper launches a new idea for the steering of probes (slow particles). In many applications steering is done by deriving the force from a potential landscape. Here we couple the probe to a nonequilibrium (driven or active) medium, and we control the frenesy, which means manipulating time-symmetric reactivities in the nonequilibrium medium. That creates or alters the mean force on the probe, for producing the wished-for trajectories. The algorithm is illustrated by steering a probe to follow the trajectories of a van der Pol oscillator and of the Lorenz system. That novel scheme has both fundamental and applied significance, as it enables to deliver controlled motion in a nonequilibrium background.

---

\*Electronic address: christian.maes@kuleuven.be

## I. INTRODUCTION

An old example of steering is encountered in irrigation networks. In the case of the Sierra Nevada, more than 3,000 km of irrigation channels were built on its slopes by the settlers of the Umayyad conquest of Hispania (8th century), [1]. The water running downhill is ingeniously diverted to flow along the different cultivations. Such controlled use of a potential (gravity in the case of surface irrigation) combined with landscaping takes a more abstract formulation in gradient flow, where descent follows a free energy profile and a local measure of distance (or metric) determines what is steepest, obtaining the gradient descent method as first proposed by Cauchy (1847), [2].

In the case of individual particles where a specific probe or collective variable is to follow a given trajectory, steering requires the more or less direct creation or alteration of the force on that probe. One way is to derive that force from a potential landscape or from a time-dependent external field. However, when the probe is coupled to a nonequilibrium medium, a newer fascinating possibility arises, the subject of the present paper.

It has indeed been realized before that violating detailed balance (breaking time-reversal symmetry) in the dynamics enables to employ kinetic aspects that otherwise remain invisible under thermal equilibrium. For instance, recent works have explored how dynamical activity, and more in particular time-symmetric reactivities, can significantly contribute to selection, recovery, or self-assembly. That includes the more recent references [3–6], but there are of course the Landauer blowtorch theorem [7, 8], or examples such as kinetic proofreading [9], that made the point much earlier.

The statistical or mean force on a probe coupled to a nonequilibrium medium is likewise influenced by time-symmetric reactivities as first shown in [10]. In the present paper, we continue that study in constructive ways: it is possible to make the probe travel basically any trajectory by correctly choosing the time-symmetric reactivities for every moment during the trajectory. In that fashion, slower dynamical degrees of freedom are steered by an underlying and faster microscopic nonequilibrium dynamics. More specifically, it will be the phase between entropy flux and frenesy that provides the steering. Such frenetic navigation offers a new tool that works away from equilibrium without the need to adapt energy landscapes. It is therefore a promising road to be explored, also within the more

general context of biological functioning. The latter is not the subject of the present paper but we sketch the broader context of control and the possible relation with bio-engines in Section V. For a broader introduction to frenesy we refer to the reviews [10, 11] and to Section V and the Appendix A more in particular.

For a more formal introduction, we still add here the main line of strategy and we explain the notion of mean force on a probe (or collective variable). The probe is slow, allowing for a quasistatic approximation where the medium is always in its *instantaneous* stationary condition. We allow the medium to be influenced by the probe's position but not by its velocity: denoting the probe position by  $x$ , the medium (only) enters through its stationary probability distribution  $\rho(x, \eta)$  where medium variables are written as  $\eta$ . Given a potential  $U(x, \eta)$  through which the medium and the probe are coupled, the induced force on the probe is:

$$f(x) = -\langle \nabla_x U(x, \eta) \rangle(x) = -\sum_{\eta} \nabla_x U(x, \eta) \rho(x, \eta) \quad (1)$$

where  $\nabla_x$  is the spatial gradient and the expectation  $\langle \cdot \rangle(x)$ , like the sum, is over the  $\eta$  (assumed discrete) for fixed  $x$ .

The dynamics of the medium is modeled using a Markov jump process. The rate to jump from  $\eta \rightarrow \eta'$  is

$$k(x, \eta, \eta') = a(x, \{\eta, \eta'\}) \exp\left(\frac{\beta}{2}(U(x, \eta) - U(x, \eta') + W(\eta, \eta'))\right) \quad (2)$$

where  $a(x, \{\eta, \eta'\}) = a(x, \{\eta', \eta\})$  is a reactivity or time-symmetric activity parameter,  $\beta = (k_B T)^{-1}$  relates to an ambient temperature  $T$ , and  $W(\eta, \eta') = -W(\eta', \eta)$  is the work done by driving forces on the medium when transiting from  $\eta$  to  $\eta'$ . The fact that  $W$  is not written as the difference of a potential indicates the nonconservative nature from which nonequilibrium features emerge.

The transition rates (2) determine the stationary probability distribution  $\rho(x, \eta)$  (assumed unique for now) for making the mean force  $f$  in (1). The main subject of the paper is to understand how to modify that force (1) by controlling the  $a(x, \{\eta, \eta'\})$  at fixed driving. That means that we do not touch the “fuel” (the nonconservative driving giving  $W$ ) or the potential  $U$  in the medium; we only manipulate the time-symmetric activities. The equation of motion of the probe is assumed here to be of the form

$$\dot{x} = f(x) \quad (3)$$

where  $x$  lives on some manifold such as the multidimensional torus or the Euclidean space. We ignore (thermal) noise. However, the main strategy of controlling the  $a(x, \{\eta, \eta'\})$  does not alter when adding other terms to (3). In particular, a phase will enter those activity parameters that varies on the time-scale of the slow variables, so that the mean force in (1) will use the instantaneous stationary probability. That can be seen as a problem of inversion as is common in control theory, [12, 13]; we must find the phase shifts in the activity parameters that create the wished-for trajectory in (3).

**Plan of the paper:** In Section II we recall a strategy to create a rotational component in the mean force. It is based on [10], and we indicate how the technique can be extended to higher dimensions as well.

Section III presents an algorithm to deterministically steer a probe. It is our main result. Other models or algorithms are conceivable but we make the idea very specific by selecting one of them.

In Section IV we apply that steering technique for reproducing the trajectories of the van der Pol oscillator and the Lorenz model.

In Section V (before the conclusions in Section VI) we come back to the general context of the paper, which allows some remarks about the connection with control theory. We also remind the reader there about the more general notion of frenesy and how it combines with control. That Section V can also be read before the more technical part starts (in the next sections).

The Appendix has four parts where we elaborate as well on possible modifications of the nonequilibrium dynamics and on details for the higher-dimensional extensions and rescaling of the force.

For the calculations we use Python [14] with the libraries Numpy[15], Matplotlib [16] and Scipy [17].

## II. GENERATING A ROTATIONAL COMPONENT IN THE MEAN FORCE

A first observation about frenetic steering was made in [10] which we repeat here in the same language and for the simplest example.

### A. On the unit circle

Suppose that the probe position is on the unit circle,  $x \in S^1$ , undergoing a mean force  $f$  defined in (1). In the present section, we restrict ourselves to the origin of the rotational part  $\oint f(x)dx$ , to produce and to indeed modify the rotation of the probe by altering time-symmetric activity parameters of the dynamics of the medium.

If the medium is in equilibrium for every position  $x$ , we get for (1) a force  $f$  which is the gradient of a potential (the free energy). More precisely, when the density  $\rho(x, \eta)$  corresponds to canonical equilibrium at inverse temperature  $\beta = (k_B T)^{-1}$  for the potential  $U(x, \eta)$  for every  $x$ , we get for the force,

$$\begin{aligned} f_{\text{eq}}(x) &= -\frac{1}{Z(x)} \sum_{\eta} \nabla_x U(x, \eta) \exp(-\beta U(x, \eta)), & Z(x) &:= \sum_{\eta} \exp(-\beta U(x, \eta)) \\ &= -\nabla_x \mathcal{F}_{\text{eq}}(x), & \mathcal{F}_{\text{eq}}(x) &:= -k_B T \log Z(x) \end{aligned}$$

where  $Z(x)$  is the canonical partition function and  $\mathcal{F}_{\text{eq}}(x)$  is the free energy. Then, the steady behavior is time-reversal symmetric and  $\oint f(x)dx = 0$  and there is no current. It implies that, to have a nonzero rotational component to the force (1), detailed balance has to be broken in the medium, but even that is not enough, as we shall now see.

To be specific about (2), we take a medium with states  $\eta = 1, 2, 3$ , and a driving  $W(x, 1, 2) = W(x, 2, 3) = W(x, 3, 1) = \varepsilon$  along the loop. The interaction potential is  $U(x, 1) = \lambda \sin x$  and  $U(x, \eta = 2, 3) = 0$ . For the reactivities in (2) we take:

$$\begin{aligned} a(x, \{1, 2\}) &= 1 + \lambda b \cos(x + \varphi), & a(x, \{1, 3\}) &= 1 - \lambda b \cos(x + \varphi) \\ a(x, \{2, 3\}) &= 1 \end{aligned} \tag{4}$$

which again contain the coupling parameter  $\lambda > 0$ , and we take an additional  $b > 0$  for changing the coupling in the reactivities. The force (1) becomes

$$f(x) = -\lambda \rho(x, 1) \cos x \tag{5}$$

The idea is to trap the system in the state  $\eta$  that provides the required force. By making  $a(x, \{1, 2\})$  small, we trap the medium in state 1, which means to increase  $\rho(x, 1)$ . For example with  $\varphi = 0$ ,  $a(x, \{1, 2\})$  is at its minimum for  $\cos x = -1$ . For those values of  $x$

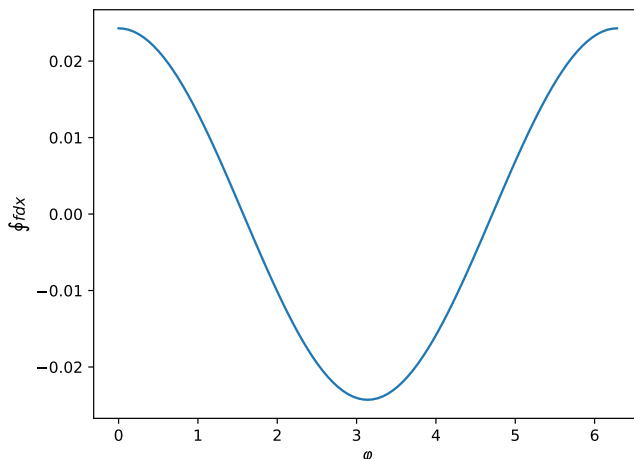


FIG. 1: The rotational part of the force for the system described around (4) with  $\beta = \varepsilon = b = 1$  and  $\lambda = 0.2$ : it turns out that  $\oint f dx \approx 0.0243 \cos \varphi$ , plotted as a function of the shift  $\varphi$ . Note in particular that  $\oint f dx = 0$  when  $\varphi = \pm\pi/2$ , *i.e.*, when the reactivities (4) are a function of the interaction energy  $U(x, \eta)$ .

the  $-\lambda \cos x$  factor in the force is maximal, so that we get a positive value for  $\oint f(x)dx$ . Manipulating the shift  $\varphi$  as a control, we can change for which values of  $x$  the reactivity  $a(x, \{1, 2\})$  is small and so influence  $\oint f(x)dx$ .

In Fig. 1 the dependence of  $\oint f(x)dx$  on  $\varphi$  is shown for  $\beta = \varepsilon = b = 1$  and  $\lambda = 0.2$ ; we see that  $\oint f(x)dx \simeq 0.0243 \cos \varphi$ . As shown in greater generality in Appendix A, to second order in  $\lambda$ , the rotational part of the force is indeed proportional to  $\cos \varphi$ . The important conclusion here is that the rotational part of the force  $\oint f(x)dx$  can be controlled with  $\varphi$ . Note that the above model can of course be run on the line  $\mathbb{R}$ , giving a periodic force  $f(x)$ , and instead of rotation, a drift to infinity. In accordance with the major conclusion in [10], and as obvious by inspecting Fig. 1, the  $x$ -dependence of the interaction energy and the  $x$ -dependence of the activity parameters must have a relevant phase difference. That shift will be the major tool for steering in what follows.

We extend the above construction in the next section to multiple dimensions (and higher-dimensional tori). Note however that the rotational part  $\oint f(x) dx$  does not completely determine the motion. That gets remedied in Section III.

## B. Multiple dimensions

We start from the same setup as above in (4) but we add equivalent terms for a second dimension with variable  $y \in S^1$ . We still have a medium with states  $\eta = 1, 2, 3$  and a driving  $W(1, 2) = W(2, 3) = W(3, 1) = \varepsilon$ , independent of  $(x, y)$ . For the energy we now take  $U(x, y, 1) = \lambda \sin x + \lambda \sin y$  and  $U(x, y, \eta = 2, 3) = 0$ . For the activity parameters we put

$$\begin{aligned} a(x, y, \{1, 2\}) &= 1 + \lambda b_x \cos(x + \varphi_x) + \lambda b_y \cos(y + \varphi_y) \\ a(x, y, \{1, 3\}) &= 1 - \lambda b_x \cos(x + \varphi_x) - \lambda b_y \cos(y + \varphi_y) \\ a(x, y, \{2, 3\}) &= 1 \end{aligned} \tag{6}$$

The force (1) then has two components

$$\begin{aligned} f_x(x, y) &= -\lambda \rho(x, y, 1) \cos x \\ f_y(x, y) &= -\lambda \rho(x, y, 1) \cos y \end{aligned}$$

Starting from results in [10], we demonstrate in Appendix B that to second order in  $\lambda$ ,  $\oint f_x(x, y) dx$  is not influenced by the  $y$ -dependencies in  $U$  or in the  $a(x, y)$ 's (including  $b_y$ ), and similarly for  $\oint f_y(x, y) dy$ . An example of that is shown in Fig. 2 where we indeed see that the influence of  $\varphi_y$  on  $\oint f_x(x, y) dx$  is limited. That means that we can control  $\oint f_x(x, y) dx$  using  $\varphi_x$  just like in the one-dimensional case without worrying that the  $y$ -dependency in  $U$  and in the  $a(x, y)$ 's would prevent us from choosing the sign of  $\oint f_x(x, y) dx$ . That obviously makes the steering much easier.

## III. STEERING THE FORCE

Turning the direction of the front wheel of a bicycle is quite useless when standing. Once in motion however, steering the bicycle becomes possible by controlling the handlebar or leaning the bike. In the following, we similarly manipulate time-symmetric aspects to create the required force.

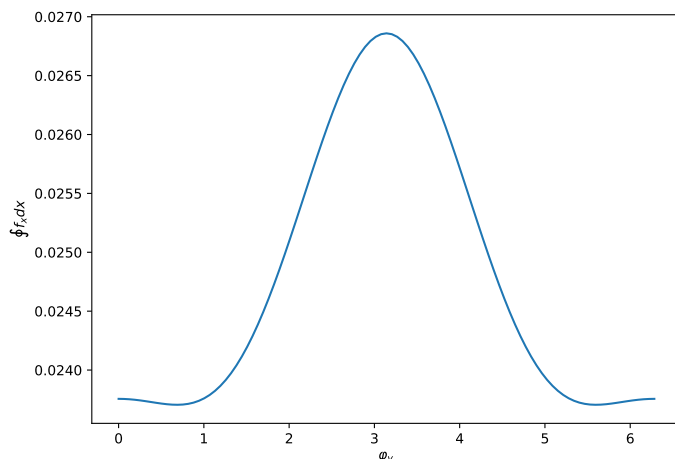


FIG. 2: The system described around (6) at  $\lambda = 0.2$ ,  $\beta = \varepsilon = b_x = b_y = 1$  and  $\varphi_x = 0$ :  $\oint f_x dx > 0$  evaluated at  $y = 0$  is almost constant as a function of  $\varphi_y$ . The variation is of order less than  $\lambda^2$ .

### A. One dimension

We start again with the situation of a probe moving on the unit circle as the result of a force induced by the interaction of the probe with a nonequilibrium medium. In the previous section, we could only control  $\oint f(x) dx$ . Now, remaining in the quasistatic approximation, ignoring fluctuations, we want to control the complete force  $f(x)$  in (1), determining the dynamics of the probe,

$$\dot{x}(t) = f(x(t)) \quad (7)$$

We choose here for an overdamped description, keeping the interpretation that  $x$  refers to a position and  $f$  is a force. That is typical for a biological context, but obviously, it can also refer to a much broader setup as used in the theory of dynamical systems (see Section IV).

It actually suffices to take 3 states in a cycle for the medium,  $\eta \in \{0, 1, 2\}$ . We refer to (2) for the structure of transition rates  $k(x, \eta, \eta')$ . There is a driving with constant magnitude  $W(0, 1) = W(1, 2) = W(2, 0) = \varepsilon$ . We use the interaction energy  $U(x, \eta) = \lambda \sin(x - \eta 2\pi/3)$  and for activity parameters we put

$$a(x, \{\eta, \eta'\}) = \begin{cases} 1 + \lambda b \cos(x - \eta 2\pi/3 + \varphi) & \text{if } \eta' - \eta \equiv 1 \pmod{3} \\ 1 + \lambda b \cos(x - (\eta - 1) 2\pi/3 + \varphi) & \text{if } \eta' - \eta \equiv 2 \pmod{3} \end{cases} \quad (8)$$



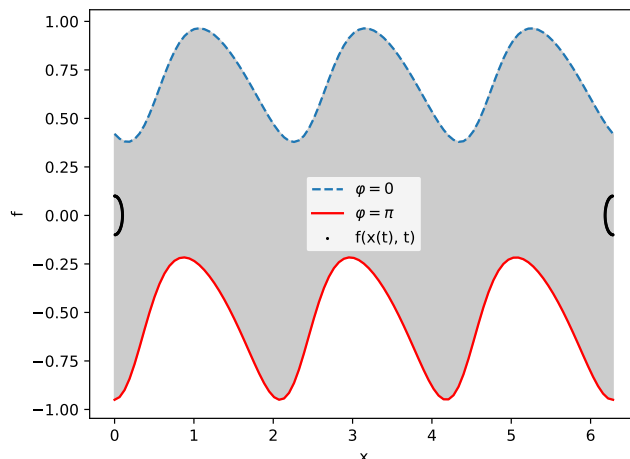


FIG. 3:  $f(x)$  for  $b = 0.99$ ,  $\lambda = 1$ ,  $\beta = 1$  and  $\varepsilon = 5$ , for  $\varphi = 0$  and  $\varphi = \pi$ . The shaded region indicates that any value of the force in that region is attainable by a suitable choice for  $\varphi$ . The black dots are values of the (time-dependent) force  $f(x(t), t)$  for the trajectory  $x(t) = 0.1 \sin(t)$  for 100 data points between  $t = 0$  and  $t = 2\pi$ .

The “shift”  $\varphi$  will control  $f(x)$  for every  $x$ .

As we see in Fig. 3, when  $\varphi = 0$  the force is positive everywhere. As for the model in Section II, that is achieved by trapping the system in the state that provides a positive force, but now the system has to be trapped in different states depending on the position. Using more than 3 states is possible. In case we use more than 3 states (when taking the same period for the sine and cosine functions) the curves in Fig. 3 would have a smaller amplitude and a smaller period. In the rest of the text we use 3 states for the model of the medium. In Appendix C we discuss results for 4 states.

Fig. 3 shows the force on the probe for  $\varphi = 0$  and  $\varphi = \pi$  depending on its position  $x$  on the circle, and for parameter values  $b = 0.99$ ,  $\lambda = 1$ ,  $\beta = 1$  and  $\varepsilon = 5$ . Depending on the shift  $\varphi$ , we can thus obtain either strictly positive or strictly negative values for that force. As it depends on  $\varphi$  in a continuous way, for every position on the circle we can also attain every value for the force between that positive and negative value. That gives a way to steer deterministically simply by controlling  $\varphi$  at preset values of (large enough)  $\varepsilon$ .

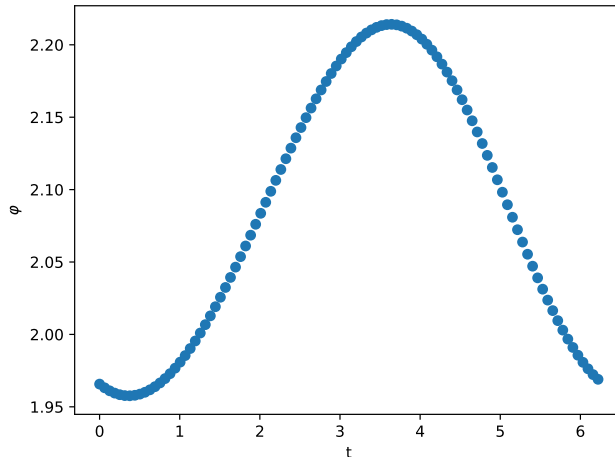


FIG. 4:  $\varphi(t)$  for the trajectory  $x(t) = 0.1 \sin(t)$  for 100 data points between  $t = 0$  and  $t = 2\pi$  and for parameter values  $b = 0.99$ ,  $\lambda = 1$ ,  $\beta = 1$  and  $\varepsilon = 5$ .

Given a trajectory  $x(t), t \in [0, T]$  for which  $\dot{x}(t)$  is between the two curves in Fig. 3, we can find  $\varphi(t)$  so that the trajectory  $x(t)$  is the result of the force on the probe induced by the medium:  $\dot{x}(t) = f(x(t), \varphi(t))$ .

As illustration, Fig. 4 shows  $\varphi(t)$  for the given trajectory  $x(t) = 0.1 \sin t$  for 100 data points between  $t = 0$  and  $t = 2\pi$ . Parameter values  $b = 0.99$ ,  $\lambda = 1$ ,  $\beta = 1$  and  $\varepsilon = 5$  were used again.  $f(x(t), t)$  for that trajectory  $x(t)$  is shown in Fig. 3, also for 100 data points between  $t = 0$  and  $t = 2\pi$ .

If  $\dot{x}(t)$  has a broader range of values (not between the two curves in Fig. 3), then we can apply a rescaling: we write  $x = Ax'$  for some  $A > 1$ , big enough, so that  $\dot{x}'(t)$  lies again between the two curves in Fig. 3, supposing that  $\dot{x}(t)$  is finite. We can then of course choose  $\varphi(t)$  for the trajectory  $x'(t)$  and retrieve  $x(t)$  from  $x'(t)$ :  $x(t) = Ax'(t)$ . Note that  $\varphi(t)$  depends on the rescaling and that that dependence is not trivial.

A second application is that given a dynamical system with equation  $\dot{x} = g(x)$ , where  $g(x)$  lies between the two curves in Fig. 3, we can find  $\varphi(x)$  so that  $f(x, \varphi(x)) = g(x)$ . If  $g(x)$  has a broader range of values, in many cases we can find an interval, say  $[x_0, x_1]$ , in which  $g(x)$  is bounded. We can then apply a rescaling  $x = Ax'$  in a similar way as above. We explain the details in Appendix D.

## B. Higher-dimensional steering

In order to steer deterministically in multiple dimensions we cannot just add the perturbations for each dimension as we did in Section II B. The appropriate extension to higher dimensions is to view the three medium states (of Section III A) as the values of a spin and to have a spin for every dimension. One could say that every spin is responsible for the force along its dimension and the spins are all independent (noninteracting). The interaction energy with the probe is additive.

Let us denote the state of the spin for dimension  $x$  as  $\eta^x$ . We take 2 dimensions for notational simplicity. We already know that the following should hold:  $\rho(x, y, \eta^x, \eta^y) = \rho(x, \eta^x)\rho(y, \eta^y)$  and

$$\begin{aligned} f_x(x, y) &= -\langle \partial_x U(x, y, \eta^x, \eta^y) \rangle(x, y) \\ &= -\langle \partial_x U_x(x, \eta^x) \rangle(x) \\ &= -\sum_{\eta^x} \partial_x U_x(x, \eta^x) \rho(x, \eta^x) \end{aligned} \quad (9)$$

but we recall the dynamics:

For 2 dimensions, we have two spins  $\eta^x, \eta^y \in \{0, 1, 2\}$ . We consider separate Markov processes for every dimension, and we use the transition rates as specified under (2) and around (8).

The two spins have the same driving (as before): e.g.,  $W_x(0, 1) = W_x(1, 2) = W_x(2, 0) = \varepsilon$  and the same for the driving on  $\eta^y$ . Both spins have an energy:  $U_x(x, \eta^x) = \lambda \sin(x - \eta^x 2\pi/3)$  and similarly for  $\eta^y$  and the interaction energy with the probe is the sum  $U(x, y, \eta^x, \eta^y) = U_x(x, \eta^x) + U_y(y, \eta^y)$ . For the activity parameters, we have for the jump between values  $\eta_i^x$  and  $\eta_j^x$

$$a_x(x, \{\eta_i^x, \eta_j^x\}) = \begin{cases} 1 + \lambda b \cos(x - \eta_i^x 2\pi/3 + \varphi_x) & \text{if } \eta_j^x - \eta_i^x \equiv 1 \pmod{3} \\ 1 + \lambda b \cos(x - (\eta_i^x - 1)2\pi/3 + \varphi_x) & \text{if } \eta_j^x - \eta_i^x \equiv 2 \pmod{3} \end{cases} \quad (10)$$

and again similarly for  $\eta^y$ .

Given a trajectory  $(x(t), y(t)), t \in [0, T]$ , we find  $\varphi_x(t)$  and  $\varphi_y(t)$  independently and in the same way as in one dimension, by requiring  $\dot{x}(t) = f_x(x(t), \varphi_x(t))$  and  $\dot{y}(t) = f_y(y(t), \varphi_y(t))$ . In other words, given a required force at a certain position  $(x, y)$  with components  $g_x(x, y)$

and  $g_y(x, y)$ , we find  $\varphi_x(x, y)$  and  $\varphi_y(x, y)$  independently in the same way as in one dimension with  $f_x(x, \varphi_x(x, y)) = g_x(x, y)$  and  $f_y(y, \varphi_y(x, y)) = g_y(x, y)$ .

There remains the issue that rescaling may be needed depending on the range of the force.

#### IV. ILLUSTRATIONS

When the medium is in equilibrium and there is a fixed interaction potential  $U(x, \eta)$ , then the force is fixed and conservative:  $f(x) = -\nabla_x \mathcal{F}_{\text{eq}}(x)$ . This seriously limits the possibilities for systems where the force is modeled as the force induced by the interaction of a probe with an equilibrium medium. When the medium is nonequilibrium the force can be nonconservative and additionally it is not completely determined by the interaction potential  $U(x, \eta)$ ; we can modify the time-symmetric activity parameters of the dynamics of the medium to depend on the position  $x$  and time.

In Section III we have introduced a model for the medium where we altered the time-symmetric activity parameters by means of the shift  $\varphi$ ; see (10). In what follows we use that algorithm to reproduce the dynamics of the van der Pol oscillator and the Lorenz system. That is achieved by using the 3-state cycle model described in Section III, where we always employ parameter values  $b = 0.99$ ,  $\lambda = 1$ ,  $\beta = 1$  and  $\varepsilon = 5$ .

Say for two dimensions like for the van der Pol oscillator, we start from given equations of motion,

$$\begin{aligned}\dot{x} &= g_x(x, y) \\ \dot{y} &= g_y(x, y)\end{aligned}\tag{11}$$

For the probe to follow that evolution, we use two approaches.

In the first approach, we select a region of state space on which we put a discrete grid. For all points  $(x_g, y_g)$  in the grid, we calculate  $\varphi_x$  so that  $f_x(x, \varphi_x(x_g, y_g)) = g_x(x_g, y_g)$  and similarly for  $\varphi_y$ . Then, given  $(x, y)$ , we find the nearest grid point  $(x_g, y_g)$  and get  $\varphi_x(x_g, y_g), \varphi_y(x_g, y_g)$ , after which we calculate  $f_x(x, \varphi_x(x_g, y_g))$  and  $f_y(y, \varphi_y(x_g, y_g))$ , which would be good approximations to  $g_x(x, y)$  and  $g_y(x, y)$ .

In the second approach we numerically integrate the equations (11) for  $t \in [0, T]$  given  $x(0)$  and  $y(0)$  and for each time step we calculate  $\varphi_x(t)$  so that  $f_x(x(t), \varphi_x(t)) = g_x(x(t), y(t))$

and similarly for  $\varphi_y(t)$ . That way our nonequilibrium model produces approximately the same trajectory for the same  $x(0)$  and  $y(0)$  as the dynamical system.

For both these approaches it is possible to use a parameterized functional form for  $\varphi_x$  and  $\varphi_y$  so that a fitting procedure would drastically decrease the storage of data.

Generalizing to an arbitrary number of dimensions is straightforward.

### A. van der Pol oscillator

The equations for the van der Pol oscillator [18, 19] are

$$\begin{aligned} \dot{x} &= y \\ \dot{y} &= -\mu(x^2 - 1)y - x \end{aligned} \tag{12}$$

modeling oscillations with nonlinear damping and amplification. It was originally (and is still) used in the context of electric activity, in particular in biological systems [20].

We take  $\mu = 1.5$ , and the region  $[-4, 4] \times [-4, 4]$ , for which the rescaling  $A = 500$  is appropriate. We use 1000 grid points in both dimensions giving a total of  $10^6$  grid points. Using the dynamics with transition rates described in (2), (8) and (10), we plot a trajectory for initial state  $x = 3, y = 0$ , time step 0.01 and duration  $T = 12$ , shown in Fig. 5. That is exactly what we expect that trajectory to look like for the van der Pol oscillator. The shifts  $\varphi_x(t)$  and  $\varphi_y(t)$  calculated for the same values for the parameters (so for initial state  $x = 3, y = 0$ , time step 0.01 and  $T = 12$ ) are shown in Fig. 6.

If  $\mu = 0$ , the solution would be  $x(t) = 3 \cos(t)$  and so a translation and rescaling of the trajectory  $x(t)$  for which  $\varphi(t)$  is shown in Fig. 4 (rescaling not only because of the amplitude of  $x(t)$  but also because of  $A = 500$ ). Because  $x(t)$  for which  $\varphi(t)$  is shown in Fig. 4 is on a different scale as  $x(t) = 3 \cos(t)$  (with rescaling  $A = 500$ ) there is however a big difference in the range of  $\varphi(t)$ .

### B. Lorenz model

The 60-year-old Lorenz system [18, 21] is particularly relevant for our purposes because it is (already) a reduced version of a larger system, [22]. The derivation, called Ober-

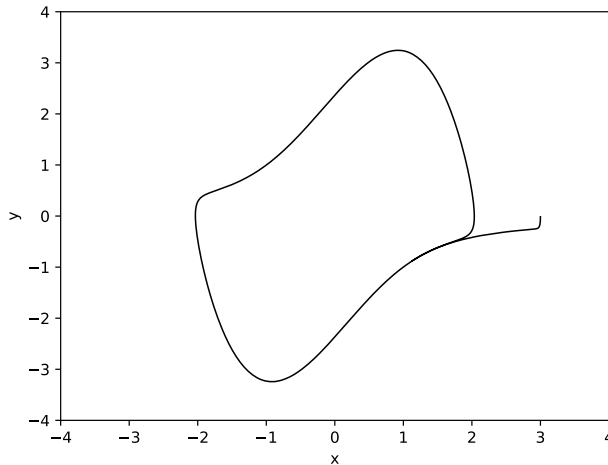


FIG. 5: A trajectory for a probe that approximates the van der Pol oscillator, for damping  $\mu = 1.5$ , initial state  $x = 3, y = 0$ , time step 0.01 and duration  $T = 12$ .

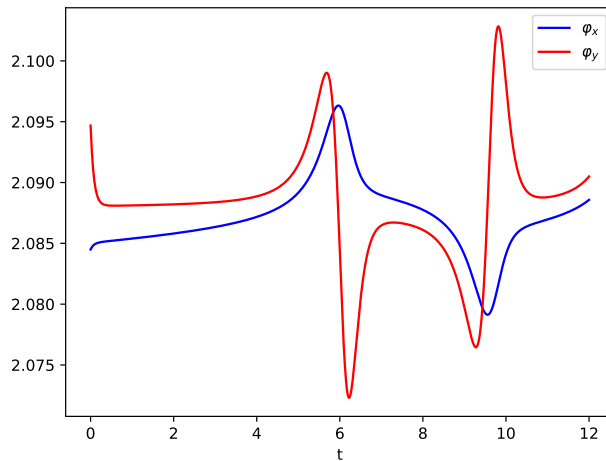


FIG. 6: Phase shifts  $\varphi_x(t)$  and  $\varphi_y(t)$  for the medium dynamics coupled to the probe that follows the van der Pol oscillator, for  $\mu = 1.5$ , initial state  $x = 3, y = 0$ , and time step 0.01.

beck–Boussinesq approximation, starts from the equations of irreversible thermo- and hydrodynamics, in particular incorporating the phenomenon of Rayleigh–Bénard convection. In the end, using a spectral Galerkin approximation, a set of three coupled, nonlinear ordinary differential equations are obtained, called the Lorenz equations for the real variables

$(x, y, z)$ ,

$$\begin{aligned}\dot{x} &= \sigma(y - x) \\ \dot{y} &= rx - y - xz \\ \dot{z} &= xy - bz\end{aligned}\tag{13}$$

The physics derivation is included in texts such as [23–25]. Our frenetic steering is obviously also using a reduced description, a much simpler but artificial one. We ignore to what extent the parameters  $\sigma$ ,  $r$  or  $b$  pick up frenetic features in the atmospheric dynamics.

We take  $\sigma = 10$ ,  $r = 28$ ,  $b = 8/3$  and the region  $[-25, 25] \times [-25, 25] \times [0, 55]$ , for which the rescaling  $A = 3700$  is appropriate. We use 1000 grid points in each direction, making  $10^9$  grid points in total. In the case of the van der Pol oscillator, which has two dimensions, it was possible to store all the values for  $\varphi_x(x, y)$  and  $\varphi_y(x, y)$  for all grid points in memory. In the case of the Lorenz model, which has three dimensions, all this data would have a size of around 80 GB, which exceeds the memory of most PC's. In order to deal with that problem, we determine the nearest grid point and its values for  $\dot{x}$ ,  $\dot{y}$ ,  $\dot{z}$  as given by (13).

Using the dynamics provided by our nonequilibrium medium (around (8), as extension to three dimensions of (10)), a trajectory  $x(t), z(t)$  for initial state  $x = 0$ ,  $y = 1$ ,  $z = 0$ , time step 0.001 and  $T = 50$  is plotted in Fig. 7(b), next to Fig. 7(a) where we see the trajectory for the same parameters but calculated from (13), exhibiting the typical Lorenz butterfly for its strange attractor, [26]. Despite some local differences, not very surprising for a dynamics that exhibits chaos, the global features are perfectly reproduced.

In Fig. 8 the shifts  $\varphi_x(t)$  and  $\varphi_z(t)$  are shown for the same values for the parameters (initial state  $x = 0$ ,  $y = 1$ ,  $z = 0$ , time step 0.001 and  $T = 50$ ). The (irregular) oscillations reproduce the chaotic nature of the trajectories  $x(t)$  and  $z(t)$ .

## V. FRENETIC STEERING AND CONTROL THEORY

The present section collects some further thoughts on frenetic control and broadens the context for a better understanding of the specific nature of the applied schemes.

Steering is an extended control, which wants to produce (as time evolves) the required trajectory, not just a final condition. Nevertheless, the present paper can be situated

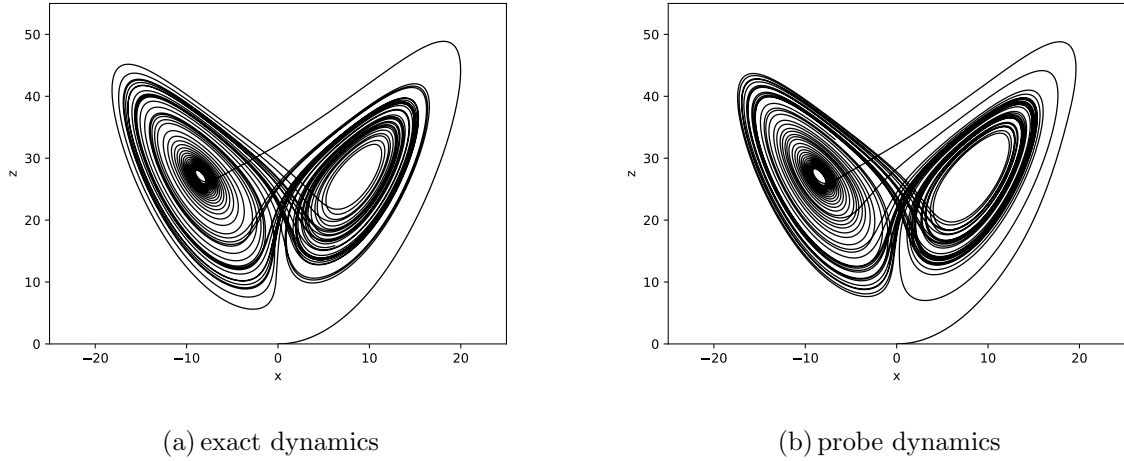


FIG. 7: Trajectories  $(x(t), z(t))$  using the exact dynamics (in (a)) and the approximated dynamics given by our nonequilibrium model (in (b)), for initial state  $x = 0$ ,  $y = 1$ ,  $z = 0$ , time step 0.001 and duration  $T = 50$ .

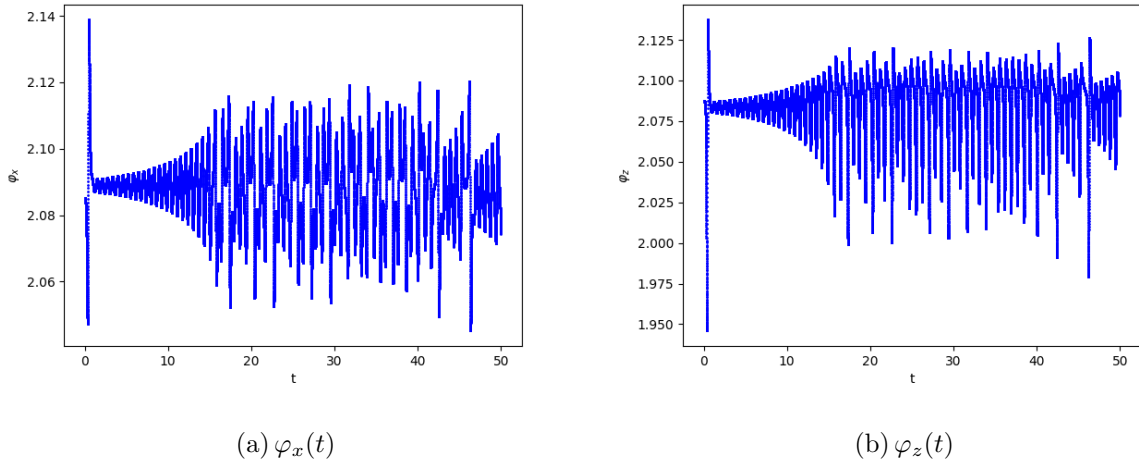


FIG. 8:  $\varphi_x(t)$ (a) and  $\varphi_z(t)$ (b) for a dynamics based on our nonequilibrium model that approximates the Lorenz model, for initial state  $x = 0$ ,  $y = 1$ ,  $z = 0$ , time step 0.001 and  $T = 50$ .

under the general heading of control theory. The latter searches for algorithms to engineer the required inputs that drive the system from some initial state(s) to a desired state or condition. Often, many constraints exist, having to do with costs, errors, time, and stability, which then define the aim to achieve a good degree of optimality. There is a multitude of methods and approaches; see *e.g.* [12] for a general physics discussion. From the latter perspective, control theory indeed combines statistical thermodynamics with the



theory of dynamical systems.

Control is typically nonconservative. The control or stimulus (such as the input current) gives rise to the dissipation of the used energy. Moreover, in a more direct sense, the control can itself use nonconservative forces which makes it a driving scheme, and subject of nonlinear and nonequilibrium response studies. The nonlinearity is present in applied feedback mechanisms but appears also from the very nature of the “control solution” which amounts to an inversion of the required response. There is no guarantee that such an inversion works; in fact, it may not be possible. In the present paper, it is accomplished via a phase shift. In control theory, “differential flatness” is often used as a condition for making the inversion possible, [13]. We have not studied how that flatness condition relates to our solution with the phase shift.

The present paper differs from standard control algorithms in a number of ways. First of all, we employ a stochastic process as stimulus. A Markov jump process is coupled to the probe. We do use nonconservative driving in the jumps but not as control. Our scheme is only *enabled* by the driving but the steering wheel is frenetic; *i.e.*, *tunes* time-symmetric reactivities.

Frenesy is a quantity that is complementary to entropy. It captures the idea of a time-symmetric dynamical activity and in that sense contrasts with fluxes or currents that have a (time-) direction. In the case of Markov jump processes, as we use in the present paper, the frenesy is made from the escape rates and the time-symmetric part of the reactivities. They are controlled by the symmetric parameters  $a(x, \{\eta, \eta'\})$  in (2). As mentioned in the introduction, it has been observed before that population and current selection can be achieved by their modulation when the nonequilibrium amplitude is high enough; see [4, 11, 27, 28]. The present paper extends that idea to steering, which is a selection mechanism on the level of trajectories (for a probe).

One can ask here for (experimental) realizations. We believe that the presented program naturally leads to a construction plan for bio(mimetic)-engines. After all, locomotion, contraction or biological work more generally, are produced via the coupling of probes (*e.g.* flagella) to nonequilibrium (sub)systems (*e.g.* molecular motors). That is exactly our scheme where the driven Markov jump process, representing agitated molecules, is coupled to a much

slower passive probe. A recent example of such a construction can be followed in [29].

Not all biological steering is frenetic but the novelty of our idea is to at least complement the use of external field protocols and of the tuned driving over energy landscapes with the possibility of changing the occupation statistics and hence the mean force via modulation of time-symmetric quantities.

## VI. CONCLUSION

Frenetic steering refers to the manipulation of parameters appearing in time-symmetric activity functions. It is applicable for a slow probe or collective variable coupled to a nonequilibrium medium where it adds the ability to manufacture forces. As a matter of fact, the parameterization can be done via a phase shift variable, which creates a twist between the variable entropy fluxes and the excess dynamical activity or frenesy.

Various algorithms are possible, and we have selected just one that works well. We have explained the general principle, and how to make it work in a multidimensional setting. We have illustrated how to guide a probe to *simulate* the van der Pol cycle and Lorenz butterfly. All that is obviously impossible for an equilibrium environment where the induced mean force on the system variables is always the gradient of a potential; guiding a probe or collective variable along a given trajectory requires coupling it with a nonequilibrium medium.

The idea may have more applications but also points to extra flexibility in active or living processes: controlling the time-symmetric fluctuation sector is a viable way to steer toward greater fitness, away from damage or even extinction. No need to update the landscape of free energies, but for a given driving or fuelling, the creation or modifications of phase shifts between entropy fluxes and frenesy may adapt functionalities to a changing environment.

## VII. DATA AVAILABILITY

Data are freely and directly available upon simple request from the authors.

### Appendix A: Shift and amplitude dependence

Consider the situation of a probe on the unit circle coupled to a nonequilibrium medium, whose state is denoted by  $\eta$ , with a small coupling parameter  $\lambda$ . Suppose we have a dynamics for the medium with a potential  $U_\lambda(x, \eta) = U_0(\eta) + \lambda U_I(x, \eta)$  where  $U_I(x, \eta) = h(\eta) \sin x$ , a nonequilibrium driving  $W(\eta_i, \eta_j)$  between every two states  $\eta_i, \eta_j$  that is independent of  $x$  and where the activity parameters are

$$a_\lambda(x, \{\eta_i, \eta_j\}) = a_0(\{\eta_i, \eta_j\}) + \lambda b(\{\eta_i, \eta_j\}) \cos(x + \varphi) \quad (\text{A1})$$

where  $\varphi$  is the same for every transition. The rates are then

$$k(x, \eta_i, \eta_j) = a_\lambda(x, \{\eta_i, \eta_j\}) \exp\left(\frac{\beta}{2}(U_\lambda(x, \eta_i) - U_\lambda(x, \eta_j) + W(\eta_i, \eta_j))\right) \quad (\text{A2})$$

We view the dynamics as a perturbation with respect to the dynamics at  $\lambda = 0$ . We show that to second order in  $\lambda$ :  $\oint f(x) dx \propto \cos \varphi$ . We use the result from [10] that the nongradient part of the force can be written as

$$f^{\text{neq}}(x) = -\frac{1}{\beta} \langle (D^\lambda - D^0) \nabla_x (S^\lambda - S^0) \rangle^0 + O(\lambda^3) \quad (\text{A3})$$

The expectation is here over paths and we consider the system in its steady state again.  $D$  is the frenesy and  $S$  is the entropy flux, both functions of the path; see [11]. The superscript  $\lambda$  signifies that the quantity is taken for the perturbed dynamics, and the superscript 0 indicates the unperturbed dynamics.  $D^\lambda - D^0$  depends on a path  $\omega$  as

$$\begin{aligned} (D^\lambda - D^0)(\omega) = & \int_0^t ds \sum_{\eta \neq \eta(s)} \exp\left(\frac{\beta}{2}(U_0(\eta(s)) - U_0(\eta) + W(\eta(s), \eta))\right) \quad (\text{A4}) \\ & \left[ (a(\{\eta(s), \eta\}) + \lambda b(\{\eta(s), \eta\}) \cos(x + \varphi)) \exp\left(\lambda \frac{\beta}{2}(U_I(x, \eta(s)) - U_I(x, \eta))\right) \right. \\ & \left. - a(\eta(s), \eta) \right] - \sum_s \log\left(1 + \lambda \frac{b(\{\eta(s^-), \eta(s)\})}{a(\{\eta(s^-), \eta(s)\})} \cos(x + \varphi)\right) \end{aligned}$$

where the sum over  $s$  is a sum over the jump times. Upon expanding to first order in  $\lambda$  and inserting the expression for  $U_I(x, \eta)$ , we get

$$\begin{aligned} (D^\lambda - D^0)(\omega) = & \lambda \int_0^t ds \sum_{\eta \neq \eta(s)} \exp\left(\frac{\beta}{2}(U_0(\eta(s)) - U_0(\eta) + W(\eta(s), \eta))\right) \\ & \left[ (a(\{\eta(s), \eta\}) \frac{\beta}{2} (h(\eta(s)) - h(\eta)) \sin x + b(\{\eta(s), \eta\}) \cos(x + \varphi)) \right] \\ & - \lambda \sum_s \frac{b(\{\eta(s^-), \eta(s)\})}{a(\{\eta(s^-), \eta(s)\})} \cos(x + \varphi) \end{aligned}$$

$(S^\lambda - S^0)(\omega)$  has a much simpler form,

$$(S^\lambda - S^0)(\omega) = \lambda\beta\left(\sum_s h(\eta(s^-)) - h(\eta(s))\right) \sin x = \lambda\beta(h(\eta(0)) - h(\eta(t))) \sin x \quad (\text{A5})$$

and so

$$\nabla_x(S^\lambda - S^0)(\omega) = \lambda\beta(h(\eta(0)) - h(\eta(t))) \cos x \quad (\text{A6})$$

To calculate  $\oint f^{\text{neq}}(x)dx$ . we switch the expectation operation and the integral over  $x$ . Then, for small  $\lambda$ , to order  $\lambda^2$ ,

$$\begin{aligned} & -\frac{1}{\beta} \oint dx (D^\lambda - D^0)(\omega) \nabla_x (S^\lambda - S^0)(\omega) = \quad (\text{A7}) \\ & -\lambda^2 \int_0^t ds \oint dx \sum_{\eta \neq \eta(s)} \exp\left(\frac{\beta}{2}(U_0(\eta(s)) - U_0(\eta) + W(\eta(s), \eta))\right) \\ & \left[ a(\{\eta(s), \eta\}) \frac{\beta}{2} (h(\eta(s)) - h(\eta)) \sin x + b(\{\eta(s), \eta\}) \cos(x + \varphi) \right] \\ & (h(\eta(0)) - h(\eta(t))) \cos x \\ & + \lambda^2 \oint dx \sum_s \frac{b(\{\eta(s^-), \eta(s)\})}{a(\{\eta(s^-), \eta(s)\})} \cos(x + \varphi) (h(\eta(0)) - h(\eta(t))) \cos x \end{aligned}$$

Using the sum formulæ for sine and cosine,

$$\begin{aligned} & -\frac{1}{\beta} \oint dx (D^\lambda - D^0)(\omega) \nabla_x (S^\lambda - S^0)(\omega) = \quad (\text{A8}) \\ & -\lambda^2 \pi \cos \varphi \int_0^t ds \sum_{\eta \neq \eta(s)} \exp\left(\frac{\beta}{2}(U_0(\eta(s)) - U_0(\eta) + W(\eta(s), \eta))\right) \\ & b(\{\eta(s), \eta\}) (h(\eta(0)) - h(\eta(t))) \\ & + \lambda^2 \pi \cos \varphi \sum_s \frac{b(\{\eta(s^-), \eta(s)\})}{a(\{\eta(s^-), \eta(s)\})} (h(\eta(0)) - h(\eta(t))) \end{aligned}$$

to order  $\lambda^2$ . Since that is true for every path  $\omega$ , it shows that  $\oint f^{\text{neq}}(x)dx \propto \cos \varphi$  to second order in  $\lambda$ . Furthermore, from this formula, we also see that multiplying  $b$  with the same factor  $d$  for all transitions,  $\oint f^{\text{neq}}(x) dx$  to second order in  $\lambda$  is multiplied by  $d$  as well.

## Appendix B: Reduction of the multi-dimensional case to one dimension

Suppose that the probe lives on a higher-dimensional torus,  $x \in T^n$ . The idea is to perturb the reactivities and the energy in an additive way over the different dimensions. We can freely choose the rotational part for every dimension. We show it here for  $n = 2$

dimensions, but it generalizes to an arbitrary number of dimensions.

Let us take the potential

$$U_\lambda(x, y, \eta) = U_0(\eta) + \lambda h_x(\eta) \sin x + \lambda h_y(\eta) \sin y \quad (\text{B1})$$

and activity parameters,

$$a_\lambda(x, y, \{\eta_i, \eta_j\}) = a_0(\{\eta_i, \eta_j\}) + \lambda b_x(\{\eta_i, \eta_j\}) \cos(x + \varphi_x) + \lambda b_y(\{\eta_i, \eta_j\}) \cos(y + \varphi_y) \quad (\text{B2})$$

and also again a nonequilibrium driving  $W(\eta_i, \eta_j)$  between every two states  $\eta_i, \eta_j$  that is independent of  $x$  and  $y$ . We use (A3) again, now to calculate  $\oint f_x(x, y) dx$ . The case  $\oint f_y(x, y) dy$  is completely analogous. Now, for  $(D^\lambda - D^0)(\omega)$  to first order in  $\lambda$ :

$$\begin{aligned} (D^\lambda - D^0)(\omega) &= \lambda \int_0^t ds \sum_{\eta \neq \eta(s)} \exp\left(\frac{\beta}{2}(U_0(\eta(s)) - U_0(\eta) + W(\eta(s), \eta))\right) \quad (\text{B3}) \\ &\left[ (a(\{\eta(s), \eta\}) \frac{\beta}{2} ((h_x(\eta(s)) - h_x(\eta)) \sin x + (h_y(\eta(s)) - h_y(\eta)) \sin y) + \right. \\ &\quad \left. b_x(\{\eta(s), \eta\}) \cos(x + \varphi_x) + b_y(\{\eta(s), \eta\}) \cos(y + \varphi_y) \right] \\ &- \lambda \sum_s \frac{b_x(\{\eta(s^-), \eta(s)\})}{a(\{\eta(s^-), \eta(s)\})} \cos(x + \varphi_x) - \lambda \sum_s \frac{b_y(\{\eta(s^-), \eta(s)\})}{a(\{\eta(s^-), \eta(s)\})} \cos(y + \varphi_y) \end{aligned}$$

and

$$\partial(S^\lambda - S^0)(\omega)/\partial x = \lambda \beta (h_x(\eta(0)) - h_x(\eta(t))) \cos x \quad (\text{B4})$$

$$\partial(S^\lambda - S^0)(\omega)/\partial y = \lambda \beta (h_y(\eta(0)) - h_y(\eta(t))) \cos y$$

We calculate  $\oint f_x^{\text{neq}}(x, y) dx$ ; the result for the other dimensions is analogous. Let us again switch the expectation with the integral, and work to second order in  $\lambda$ ,

$$\begin{aligned} &-\frac{1}{\beta} \oint dx (D^\lambda - D^0)(\omega) \partial(S^\lambda - S^0)(\omega)/\partial x = \quad (\text{B5}) \\ &-\lambda^2 \int_0^t ds \oint dx \sum_{\eta \neq \eta(s)} \exp\left(\frac{\beta}{2}(U_0(\eta(s)) - U_0(\eta) + W(\eta(s), \eta))\right) \\ &\left[ a(\{\eta(s), \eta\}) \frac{\beta}{2} ((h_x(\eta(s)) - h_x(\eta)) \sin x + (h_y(\eta(s)) - h_y(\eta)) \sin y) \right. \\ &\quad \left. + b_x(\{\eta(s), \eta\}) \cos(x + \varphi_x) + b_y(\{\eta(s), \eta\}) \cos(y + \varphi_y) \right] (h_x(\eta(0)) - h_x(\eta(t))) \cos x \\ &+ \lambda^2 \oint dx \sum_s \frac{b_x(\{\eta(s^-), \eta(s)\})}{a(\{\eta(s^-), \eta(s)\})} \cos(x + \varphi_x) (h_x(\eta(0)) - h_x(\eta(t))) \cos x \\ &+ \lambda^2 \oint dx \sum_s \frac{b_y(\{\eta(s^-), \eta(s)\})}{a(\{\eta(s^-), \eta(s)\})} \cos(y + \varphi_y) (h_x(\eta(0)) - h_x(\eta(t))) \cos x \end{aligned}$$

Using again the sum rules for sine and cosine,

$$\begin{aligned}
& -\frac{1}{\beta} \oint dx (D^\lambda - D^0)(\omega) \partial(S^\lambda - S^0)(\omega) / \partial x = \tag{B6} \\
& -\lambda^2 \cos(\varphi_x) \pi \int_0^t ds \sum_{\eta \neq \eta(s)} \exp\left(\frac{\beta}{2}(U_0(\eta(s)) - U_0(\eta) + W(\eta(s), \eta))\right) \\
& \quad b_x(\{\eta(s), \eta\})(h_x(\eta(0)) - h_x(\eta(t))) \\
& + \lambda^2 \cos(\varphi_x) \pi \sum_s \frac{b_x(\{\eta(s^-), \eta(s)\})}{a(\{\eta(s^-), \eta(s)\})} (h_x(\eta(0)) - h_x(\eta(t)))
\end{aligned}$$

to order  $\lambda^2$ . All terms involving  $y$  have disappeared and we can control  $\oint f_x(x, y) dx$  via  $\varphi_x$ , to second order in  $\lambda$ , as in the one-dimensional case, as if there were no perturbations in the second  $y$ -dimension.

### Appendix C: Using a four-state nonequilibrium medium

We can wonder whether the steering performance increases when including more states in the nonequilibrium medium, or when increasing the driving amplitude more. The answer is that the forces that can be obtained remain of the same order, and that the dependence on the driving saturates as well. Here we illustrate the case using a nonequilibrium medium with 4 instead of 3 states, described around (8). We discuss similarities and some differences.

The nonequilibrium model with 4 states is a straightforward adaptation of the model with 3 states described around (8) to 4 states. We describe the dynamics here. We now have  $\eta \in \{0, 1, 2, 3\}$ . The transition rates  $k_x(\eta, \eta')$  are still given by (2). There is a driving with constant magnitude  $W(0, 1) = W(1, 2) = W(2, 3) = W(3, 0) = \varepsilon$ . For the interaction energy we now have  $U(x, \eta) = \lambda \sin(x - \eta\pi/2)$  and for the activity parameters:

$$a(x, \{\eta, \eta'\}) = \begin{cases} 1 + \lambda b \cos(x - \eta\pi/2 + \varphi) & \text{if } \eta' - \eta \equiv 1 \pmod{4} \\ 1 + \lambda b \cos(x - (\eta - 1)\pi/2 + \varphi) & \text{if } \eta' - \eta \equiv 3 \pmod{4} \end{cases} \tag{C1}$$

When  $\eta' - \eta \equiv 2 \pmod{4}$ ,  $a(x, \{\eta, \eta'\}) = 0$  because the states are on a cycle.

Fig. 9 shows the force for  $\varphi = 0$  and  $\varphi = \pi$  depending on the position  $x$ , using parameter values  $b = 0.99$ ,  $\lambda = 1$ ,  $\beta = 1$  and  $\varepsilon = 5$ . Indeed the curves have a smaller amplitude and a smaller period than in Fig. 3. Here we have 4 instead of 3 peaks for both curves.

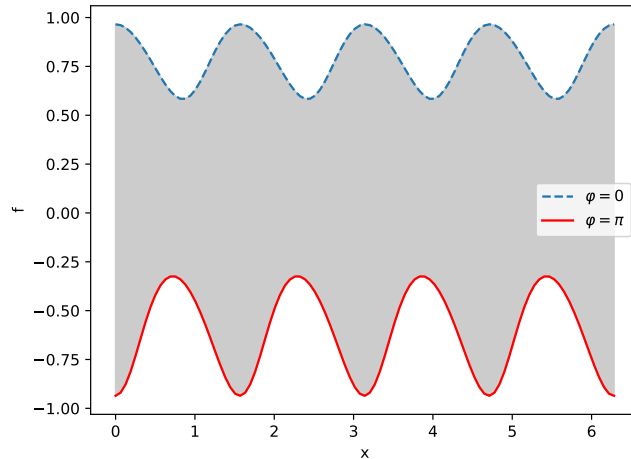


FIG. 9: The force  $f(x)$  for  $b = 0.99$ ,  $\lambda = 1$ ,  $\beta = 1$  and  $\varepsilon = 5$ , for  $\varphi = 0$  and  $\varphi = \pi$  in the nonequilibrium model with 4 states. The shaded region indicates that any value of the force in that region is attainable by a suitable choice for  $\varphi$ .

Fig. 10 shows  $\varphi(t)$  for the given trajectory  $x(t) = 0.1 \sin t$  for 100 data points between  $t = 0$  and  $t = 2\pi$ . Parameter values  $b = 0.99$ ,  $\lambda = 1$ ,  $\beta = 1$  and  $\varepsilon = 5$  were used again. The two jumps in the value for  $\varphi$  (*e.g.*, from around 1.6 to around 1.9) exist because  $f(x(t), \varphi(t)) = \dot{x}(t)$  has multiple solutions for  $\varphi(t)$  for some values of  $x(t)$  and  $\dot{x}(t)$ , and the algorithm can jump to the other solution (and in some cases has no other choice because for some values of  $x(t)$  and  $\dot{x}(t)$  there is only one solution for  $\varphi(t)$ ). Aside from the fact that there are no jumps in the value for  $\varphi(t)$ , the curve in Fig. 10 has the same overall shape as the curve in Fig. 4: they are both concave and attain their maximal value at  $t$  a little bit smaller than 4. This is undoubtedly due to the models being very similar. The dependence of the potential  $U$  and the activity parameters  $a$  on the slow macroscopic degrees of freedom, the states of the nonequilibrium medium and the phase shifts is very similar; the difference lies only in the number of ‘steps’ there are.

Let us now move to the illustrations in Section IV.

The first thing to say is that there is no change in the actual trajectories, *i.e.*, Fig. 5 and Fig. 7(b) do not change when using 4 states in the nonequilibrium medium. The point is that the grid used to approximate the dynamics is exactly the same. It does not

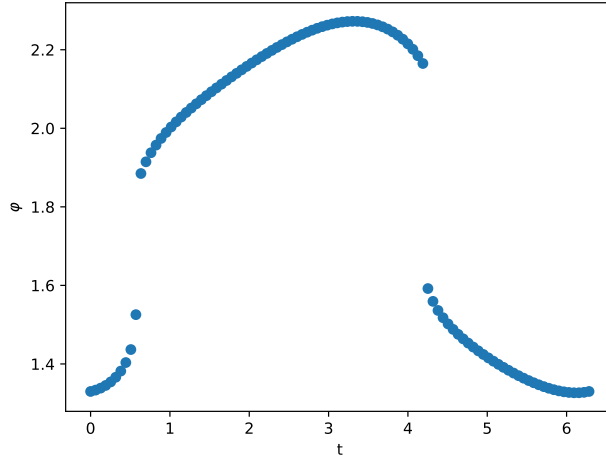


FIG. 10: The shift  $\varphi(t)$  to reproduce the trajectory  $x(t) = 0.1 \sin t$ , using 100 data points between  $t = 0$  and  $t = 2\pi$  and for parameter values  $b = 0.99$ ,  $\lambda = 1$ ,  $\beta = 1$  and  $\varepsilon = 5$  for the nonequilibrium model with 4 states.

matter that the time-derivative of the slow macroscopic variable is determined by the 3-state or the 4-state model for the medium. For all grid points the result is exactly the same.

What is different is the required choice of phase shifts. For the van der Pol oscillator and for the same values for the parameters, the phase shifts  $\varphi_x(t)$  and  $\varphi_y(t)$  are shown in Fig. 11. Both curves again have a similar shape as in Fig. 6 for the model with 3 states.

For the Lorenz dynamics, Fig. 12 shows the shifts  $\varphi_x(t)$  and  $\varphi_z(t)$  for a trajectory using the same parameter values as in Fig. 8. There are again similarities with the plots shown in Fig. 8, but, for the 4 state model, there are jumps in the values for  $\varphi_x(t)$  and  $\varphi_z(t)$ , like we had in Fig. 10. The values for  $\varphi$  are roughly in the range  $[1.3, 1.6] \cup [1.9, 2.2]$  so there is a gap between around 1.6 to around 1.9.

#### Appendix D: Scaling

The force that can be generated by the four-state cycle system described in Section III is bounded. Consider again the dynamical system  $\dot{x} = g(x)$ . If we can find an interval  $[x_0, x_1]$  for which  $g(x)$  is bounded, then we can do a rescaling of the system so that for the rescaled system the required force always falls between the two curves in Fig. 3. We rescale



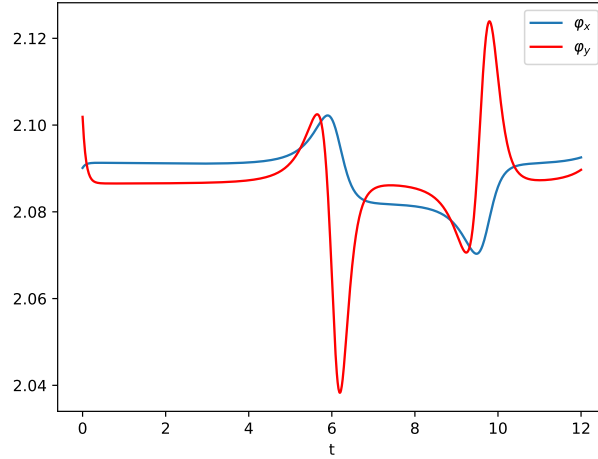


FIG. 11: Phase shifts  $\varphi_x(t)$  and  $\varphi_y(t)$  for the medium dynamics coupled to the probe that follows the van der Pol oscillator, for  $\mu = 1.5$ , initial state  $x = 3, y = 0$ , time step 0.01 and  $T = 12$  for the nonequilibrium model with 4 states.

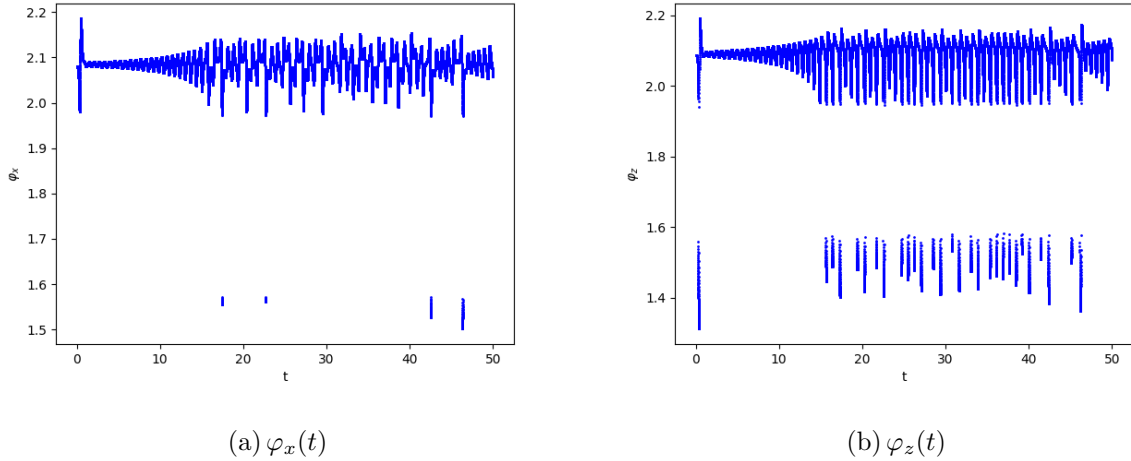


FIG. 12: Shift  $\varphi_x(t)$  and  $\varphi_z(t)$  required for simulating the Lorenz model, for initial state  $x = 0, y = 1, z = 0$ , time step 0.001 and  $T = 50$  using the nonequilibrium medium, with 4 states.

in the following way:  $x = Ax'$  for some  $A > 1$ , big enough. A good choice for  $A$  would be  $\max\{|\dot{x}| | x \in [x_0, x_1]\}/0.2$  (notice in Fig. 3 that for the curve for  $\varphi = 0$ :  $f(x) > 0.2$  and that for the curve for  $\varphi = \pi$ :  $f(x) < -0.2$ ). The rescaled system obeys

$$\dot{x}' = g'(x') = \dot{x}/A = g(x)/A \quad (\text{D1})$$

For  $x \in [x_0, x_1]$ , we can then find  $\varphi'(x')$  (we write  $\varphi'$  instead of  $\varphi$  because it is a function of  $x'$ ), so that the force generated by the medium is equal to the force required by the rescaled dynamical system:  $f(x', \varphi'(x')) = g'(x')$ . We put  $\varphi(x) = \varphi'(x')$ , and given  $\varphi'(x')$  we can for any  $x \in [x_0, x_1]$  obtain  $g(x) = Af(x', \varphi'(x'))$ . This method can be straightforwardly generalized to multiple dimensions.

- 
- [1] D. Fairchild Ruggles. *Islamic gardens and landscapes*. Penn studies in landscape architecture. University of Pennsylvania Press, Philadelphia, (2008).
- [2] Augustin-Louis Cauchy. Methode generale pour la resolution des systemes d'equations simultanees. *Comptes Rendus Hebd. Séances Acad. Sci. Paris*, 25:536–538, (1847).
- [3] Roman Belousov, Sabrina Savino, Prachiti Moghe, Takashi Hiiragi, Lamberto Rondoni, and Anna Erzberger. When time matters: Poissonian cellular potts models reveal nonequilibrium kinetics of cell sorting. *arXiv e-prints*, (2023), 2306.04443.
- [4] Christian Maes. *Non-Dissipative Effects in Nonequilibrium Systems*. Springer International Publishing AG, Cham, (2017).
- [5] Bram Lefebvre and Christian Maes. Frenetic steering in a nonequilibrium graph. *Journal of Statistical Physics*, **190**(4):90, (2023).
- [6] Ivan Di Terlizzi and Marco Baiesi. Kinetic uncertainty relation. *J. Phys. A: Math. Theor.*, **52**(2):02LT03, (2019).
- [7] Rolf Landauer. Inadequacy of entropy and entropy derivatives in characterizing the steady state. *Physical review. A, General physics*, **12**(2):636–638, (1975).
- [8] Christian Maes and Karel Netočný. Heat bounds and the blowtorch theorem. *Ann. H. Poincaré*, **14**(5):1193–1202, (2013).
- [9] John Hopfield. Kinetic proofreading: A new mechanism for reducing errors in biosynthetic processes requiring high specificity. *Proc. Natl. Acad. Sci. U.S.A.*, **71**(10):4135–4139, (1974).
- [10] Christian Maes and Karel Netočný. Nonequilibrium corrections to gradient flow. *Chaos: An Interdisciplinary Journal of Nonlinear Science*, **29**(7):073109, (2019).
- [11] Christian Maes. Frenesy: Time-symmetric dynamical activity in nonequilibria. *Physics Reports*, **850**:1–33, (2020).
- [12] John Bechhoefer. *Control Theory for Physicists*. Cambridge University Press, Cambridge, (2021).
- [13] Karl Johan. Åstrom and Richard M.. Murray. *Feedback systems: an introduction for scientists and engineers*. Princeton University Press, Princeton, second edition, (2021).
- [14] Guido Van Rossum and Fred L. Drake. *Python 3 Reference Manual*. CreateSpace, Scotts Valley, CA, (2009).

- [15] Charles R. Harris, K. Jarrod Millman, Stéfan J. van der Walt, Ralf Gommers, Pauli Virtanen, David Cournapeau, Eric Wieser, Julian Taylor, Sebastian Berg, Nathaniel J. Smith, Robert Kern, Matti Picus, Stephan Hoyer, Marten H. van Kerkwijk, Matthew Brett, Allan Haldane, Jaime Fernández del Río, Mark Wiebe, Pearu Peterson, Pierre Gérard-Marchant, Kevin Sheppard, Tyler Reddy, Warren Weckesser, Hameer Abbasi, Christoph Gohlke, and Travis E. Oliphant. Array programming with NumPy. *Nature*, 585(7825):357–362, (2020).
- [16] J. D. Hunter. Matplotlib: A 2d graphics environment. *Computing in Science & Engineering*, 9(3):90–95, (2007).
- [17] Pauli Virtanen, Ralf Gommers, Travis E. Oliphant, Matt Haberland, Tyler Reddy, David Cournapeau, Evgeni Burovski, Pearu Peterson, Warren Weckesser, Jonathan Bright, Stéfan J. van der Walt, Matthew Brett, Joshua Wilson, K. Jarrod Millman, Nikolay Mayorov, Andrew R. J. Nelson, Eric Jones, Robert Kern, Eric Larson, C J Carey, İlhan Polat, Yu Feng, Eric W. Moore, Jake VanderPlas, Denis Laxalde, Josef Perktold, Robert Cimrman, Ian Henriksen, E. A. Quintero, Charles R. Harris, Anne M. Archibald, Antônio H. Ribeiro, Fabian Pedregosa, Paul van Mulbregt, and SciPy 1.0 Contributors. SciPy 1.0: Fundamental Algorithms for Scientific Computing in Python. *Nature Methods*, 17:261–272, (2020).
- [18] Steven Strogatz. *Nonlinear Dynamics and Chaos: With Applications to Physics, Biology, Chemistry and Engineering*. Westview Press, Cambridge, 1st paperback print. edition, (2000).
- [19] Balthasar van der Pol. On “relaxation-oscillations”. *The London, Edinburgh, and Dublin Philosophical Magazine and Journal of Science*, 2(11):978–992, (1926).
- [20] Balthasar van der Pol and Jan van der Mark. The heartbeat considered as a relaxation oscillation, and an electrical model of the heart. *Philosophical Magazine*, 6(38):763–775, (1928).
- [21] Edward Lorenz. Deterministic nonperiodic flow. *Journal of Atmospheric Sciences*, 20(2):130–148, (1963).
- [22] Barry Saltzman. Finite amplitude free convection as an initial value problem—i. *Journal of Atmospheric Sciences*, 19(4):329 – 341, (1962).
- [23] Robert Hilborn. *Chaos and Nonlinear Dynamics: An Introduction for Scientists and Engineers*. Oxford University Press, New York, 2nd ed.; repr. edition, (2003).
- [24] Pierre Bergé, Yves Pomeau, and Christian Vidal. *Order within Chaos: Towards a Deterministic Approach to Turbulence*. John Wiley & Sons, New York, (1984).

- [25] Bo-Wen Shen. Nonlinear feedback in a six-dimensional lorenz model: impact of an additional heating term. *Nonlinear processes in geophysics*, **22**(6):749–764, (2015).
- [26] Warwick Tucker. A rigorous ode solver and smale’s 14th problem. *Foundations of computational mathematics*, **2**(1):53–117, (2002).
- [27] Christian Maes. What decides the direction of a current? *Mathematics and Mechanics of Complex Systems*, 4(3–4):275–295, (2016).
- [28] Urna Basu and Christian Maes. Nonequilibrium response and frenesy. *Journal of Physics: Conference Series*, 638:012001, (2015).
- [29] Faezeh Khodabandehlou and Christian Maes. Local detailed balance for active particle models. (2024), 2401.11850.